RESEARCH ARTICLE

ADVANCED OPTICAL MATERIALS
www.advopticalmat.de

Stabilizing Single-Source Evaporated Perovskites with Organic Interlayers for Amplified Spontaneous Emission

Sang-Hyun Chin, Daniele Cortecchia, Michele Forzatti, Chun-Sheng Wu, Ada Lili Alvarado-Leaños, Giulia Folpini, Antonella Treglia, Isabella Antony Kalluvila Justin, Abhyuday Paliwal, Changsoon Cho, Cristina Roldán-Carmona, Michele Sessolo, Annamaria Petrozza,* and Henk J. Bolink**

Metal halide perovskites are promising semiconductors with promising applications in optoelectronic and photonic technologies. When coherent emission applications are targeted, materials with lower lasing thresholds and increased stabilities must be developed to increase the performance under continuous wave optical pumping condition and finally allow the realization of the long sought-after electrically pumped lasers. Perovskite multiple-quantum-wells (MQWs) can potentially ease the population inversion by confining photoexcitation within the heterostructure's wells, but their fabrication process and structural design still require a delicate optimization to make them valuable photonic platforms. Here, perovskite MQWs are fabricated based on organic semiconductors and $CsPbBr_3$, using a facile and easily scalable sequential single-source vacuum evaporation method. Perovskite with the organic interlayer shows radically enhanced phase stability, passivated defects, and improved radiative recombination properties. In this way, upon proper design of the heterostructure wells and barriers thicknesses, optically pumped amplified spontaneous emission can be achieved. This work reports an effective fabrication approach for perovskite MQWs, while providing a deeper understanding of their photophysical properties to foster their application as coherent light emitters.

1. Introduction

Halide perovskites have been intensively investigated for light emission[1,2] in virtue of their excellent and tunable optoelectronic properties,[3,4] making them an attractive material platform for light-emitting diode (LED) applications as well as lasing.[2,5–11] However, important milestones such as long-term stability and the realization of electrically pumped lasing could not be realized to date, prompting the investigation of new material's engineering strategies.[7–9,12,13]

Multi-quantum-well (MQW) architectures, made of the alternation of semiconducting wells and insulating layers acting as potential barriers, can potentially increase carrier concentrations within the active layers and favor population inversion by enhancing the carrier density and electron/hole recombination rate.[14] Within the family of metal halide perovskites, 2D perovskites stand out for their layered structure made of alternating organic and

S.-H. Chin, M. Forzatti, I. A. Kalluvila Justin, A. Paliwal, C. Roldán-Carmona, M. Sessolo, H. J. Bolink
Instituto de Ciencia Molecular (ICMol)
Universidad de Valencia
C/Catedrático J. Beltrán 2, Paterna 46980, Spain
E-mail: sanghyunchin@skku.edu; henk.bolink@uv.es

The ORCID identification number(s) for the author(s) of this article can be found under https://doi.org/10.1002/adom.202302701

DOI: 10.1002/adom.202302701

S.-H. Chin
Department of Nano Science and Technology and Department of Nanoengineering
SKKU Advanced Institute of Nanotechnology (SAINT)
Sungkyunkwan University
Suwon 16419, Republic of Korea

D. Cortecchia, C.-S. Wu, A. L. Alvarado-Leaños, G. Folpini, A. Treglia, A. Petrozza
Center for Nanoscience and Technology@PoliMi
Istituto Italiano di Tecnologia
via Giovanni Pascoli 70/3, Milano 20133, Italy
E-mail: annamaria.petrozza@iit.it

D. Cortecchia
Department of Industrial Chemistry
Università di Bologna
Bologna 40136, Italy

inorganic sheets, which makes them alike self-assembled MQWs with marked excitonic properties; recent developments have demonstrated the possibility to achieve amplified spontaneous emission and low-threshold lasing up to room temperature, reviving the interest in layered perovskites for coherent emission.[15–17] Typically, these are synthesized from solution processes, relying on the self-assembly of organic and inorganic components, where the precise control of the compositional and structural parameters are critical factors for their operation. In this synthetic approach, however, steric hindrance and charge balance pose rigid constraints on the choice of materials that can be employed for the construction of MQWs architecture, and difficulties in controlling the kinetics of nucleation and crystal growth lead to phase disproportionation processes that critically compromise the formation of phase-pure structures with high dimensionality. Overall, this hampers the full optimization of internal energy level alignment of these heterostructures. An alternative approach to the realization of perovskite MQWs is their fabrication through vacuum deposition, which can greatly expand the combination of wells and barriers materials further allowing the independent tuning of their thicknesses. Surprisingly, vacuum deposited MQWs based on halide perovskite remain largely unexplored. Antrack et al. conducted an optical study with perovskite-organic MQWs and observed amplified spontaneous emission (ASE) with low threshold fluence of optical excitation following the fabrication method of Lee et al.[18–20] In that report, CsBr and $PbBr_2$ are co-evaporated to form $CsPbBr_3$ with various thicknesses (from 5 to 50 nm), while 2,2′,2′′-(1,3,5-benzinetriyl)-tris(1-phenyl-1-H-benzimidazole) (TPBi) layers of 5 nm are intercalated via thermal evaporation. However, co-evaporation of perovskite requires a highly demanding optimization. For instance, controlling evaporation rates of several precursors is difficult and following recipe of the evaporation can be less trustworthy with other evaporators since each thermal evaporator has different geometric factors due to the positions of thermal sources and sensors.[21,22] To overcome these limitations, here we report a facile fabrication strategy employing single-source evaporation with ball-milled perovskite ($CsPbBr_3$) and the photonic properties of perovskite-organic multilayers depending on the thickness of both inorganic and organic layers. We show that a TPBi cladding is crucial to stabilize the 3D $CsPbBr_3$ against the undesired $CsPb_2Br_5$ phase by contributing to reduce its microstrain. Upon optimization of the barrier layers, we find that an ideal combination of defect passivation and light confinement enhances the perovskite luminescence intensity and lowers the threshold for amplified spontaneous emission, offering fundamental insights for the optimization of easily scalable perovskite-organic multilayers toward lasing applications. The $CsPbBr_3$ perovskite powder is made by reacting CsBr and $PbBr_2$ powders via dry mechanochemical synthesis via ball-milling as per our previous reports.[23,24] The precursors are weighted stoichiometrically inside an inert N_2 filled glovebox.

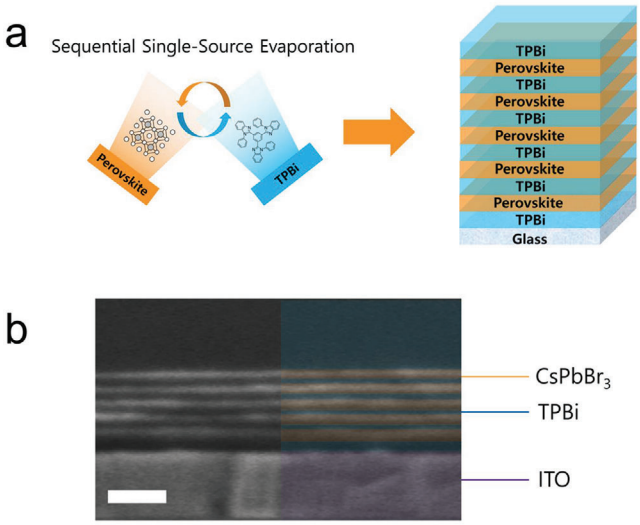

Figure 1. a) Schematic illustration of sequential single-source evaporation, an example of perovskite-organic multilayer and b) cross-section image with scanning electron microscopy (scale bar: 100 nm).

After the synthesis of the perovskite, the powder is transferred to a vacuum chamber equipped with thermal sources for the sublimation of inorganic and organic compounds. To form the perovskite-organic multilayers, $CsPbBr_3$ and TPBi are heated up to 420 and 230 °C respectively in a high vacuum, $\approx 10^{-6}$ mbar. The materials are evaporated on glass substrates and annealed at 85 °C in the nitrogen-filled glovebox, immediately after evaporation. The morphology of 100 nm-thick single source evaporated perovskite by atomic force microscpe has shown in Figure S1 (Supporting Information). The root-mean-square value of roughness ≈4 nm indicates that the film is smooth enough to eliminate harmful factor from roughness for ASE.[25,26] In addition, the freshly mechanochemically synthesized perovskite powder has been used for every experiment. The used perovskite powder shows XRD patterns from $PbBr_2$ and $CsPb_2Br_5$ as shown in Figure S2 (Supporting Information).

2. Results and Discussion

The schematic illustration of the multilayers is presented in **Figure 1a**. During the layer-by-layer evaporation, each material is individually evaporated, and the source is cooled down before starting the subsequent evaporation. After this "sequential single-source evaporation", the perovskite-organic multilayer is achieved. The process starts with the deposition of the organic layer to favor the formation of the 3D $CsPbBr_3$ perovskite film. In the absence of TPBi, the 2D $CsPb_2Br_5$ phase is found to be the dominant one, and this 2D material has a lower refractive index in the visible part of the electromagnetic spectrum.[27] The formation of the 2D $CsPb_2Br_5$ has been confirmed with X-ray diffraction (XRD) measurement (Figure S3, Supporting Information): the peak at $2\theta = 11.7°$ is characteristic of the 2D $CsPb_2Br_5$ phase, and its intensity increases upon annealing at 85 °C in the absence of the TPBi seeding layer. When TPBi is deposited on

A. L. Alvarado-Leaños, A. Treglia
Physics Department
Politecnico di Milano
Piazza Leonardo da Vinci 32, Milan 20133, Italy
C. Cho
Department of Material Science and Engineering
Pohang University of Science and Technology (POSTECH)
Pohang 36763, Republic of Korea

the glass substrate before perovskite, the peak at $2\theta = 11.7°$ is mostly suppressed and the reflection at $2\theta = 15.2°$, characteristic of 3D $CsPbBr_3$, becomes dominant. To get a deeper insight on the effects underlying this phase stabilization and unveil the effect of intercalating organic layer between perovskite and substrate, we performed the Williamson-Hall analysis based on the X-ray diffraction pattern.[28] It is well-known that size-induced and strain-induced peak broadenings vary differently as a function of Bragg angle θ,

$$\beta_{size} = \frac{K\lambda}{L\cos\theta} \tag{1}$$

$$\beta_{strain} = 4\epsilon\frac{\sin\theta}{\cos\theta} \tag{2}$$

where β_{size} and β_{strain} are size- and strain- originated broadening, respectively; K is a constant depending on crystallite shape; λ is the X-ray wavelength; L is the crystallite size; and ϵ is the "lattice micro-strain".

The Williamson–Hall method assumes that the total real sample broadening, β_{sample}, is a simple sum of the two effects, where:

$$\beta_{sample} = \beta_{size} + \beta_{strain} = \frac{K\lambda}{L\cos\theta} + 4\epsilon\frac{\sin\theta}{\cos\theta} \tag{3}$$

Multiplying throughout by cos θ gives:

$$\beta_{sample}\cos\theta = \frac{K\lambda}{L} + 4\epsilon\sin\theta \tag{4}$$

Therefore, a plot of $\beta_{sample}\cos\theta$ against $\sin\theta$ is a linear plot whereby the slope is proportional to the micro-strain ϵ and the intercept is inversely proportional to the crystallite size L. (Figure S4, Supporting Information) The X-ray diffraction patterns were fitted to a Lorentzian distribution function. The analysis shows a significant decrease of 85% (from 7.23×10^{-4} to 1.08×10^{-4}) in micro-strain of the perovskite film on the underlying organic layer, which implies that a destabilizing factor is suppressed.[29] Furthermore, the peaks shift toward higher diffraction angles after intercalation. This indicates that introducing organic layers introduces compressive strain which stabilizes the 3D phase of the perovskite. Hence, to exploit single-source evaporated $CsPbBr_3$ for coherent emission, it is recommended to introduce an organic layer between the perovskite and the substrate, since laser excitation with high fluence is required while the high refractive index of 3D $CsPbBr_3$ needs to be maintained for confinement of photon.[29]

In Figure 1b, the perovskite-organic multilayer on indium tin oxide (ITO) substrate is visualized with cross-section scanning electron microscopy (SEM). It is confirmed that TPBi layers (colored in orange) separate $CsPbBr_3$ layers (colored in blue) effectively, forming multilayer. ITO (colored in purple) is employed for SEM imaging to avoid electrical charging, however it is not used in the following optical characterization due to its high refractive index, which would cause parasitic optical loss and suppressed ASE.[30] Notably, the TPBi layers stabilize the 3D perovskite phase and leads to a ≈10-fold increase in the photoluminescence (PL) compared to the non-passivated perovskite, and also acts as the best passivating material when compared to other commonly employed organic semiconductors (Figure S5, Supporting Information), as also previously reported.[31,32]

In short, the TPBi-based organic interlayer has a dual role of seeding layer and defect passivator. As discussed before, previous reports systemically studied the photophysical properties of perovskite-TPBi MQWs.[18,19] To confirm that TPBi effectively confines evaporated $CsPbBr_3$ layers forming a MQW system, a photophysical study is conducted. For this study we prepared 5 types of MQWs with 3, 5, 10, and 60 nm-thick perovskite films, all sandwiched in between 15 nm-thick TPBi interlayers. Additionally, a 150 nm-thick perovskite film, as a reference, is prepared to investigate bulk versus multilayered films. In **Figure 2a**, a clear blue shift of the absorption spectra (from 523 to 508 nm) can be observed for films with a decreasing thickness of the perovskite layer, due to vertical quantum confinement of the perovskite between the adjacent TPBi films. The blue shift becomes more evident when the thickness is below 5 nm, which is expected as the Bohr diameter of Wannier-Mott excitons for $CsPbBr_3$ is reported to be 7 nm.[3,18] Interestingly, the absorption spectrum from the bulk reference film of 150 nm $CsPbBr_3$ shows a huge Urbach tail (67 meV, Figure S6, Supporting Information) while the MQWs with the TPBi interlayers mostly have small values, especially in the case of the 60 nm-thick $CsPbBr_3$ (18 meV). This reduced Urbach energy also proves that the organic layer interacts with the perovskite layers and passivates the defect states.[33,34] In addition, effective quantum confinement is also confirmed by the photoluminescence (PL) spectra in Figure 2b. In the 3 nm-thick film, the blue shift is 17 nm in comparison with the PL of a 150 nm perovskite film. The variation of the energy at the maximum PL with the perovskite layer thickness is depicted (Figure 2b). The steady state PL of quantum confined perovskites has been previously investigated, mostly with nanostructured $CH_3NH_3PbBr_3$ perovskites blended with organic materials such as 4,4-bis(N-carbazolyl)−1,1-biphenyl (CBP) or excess CH_3NH_3Br.[4,35] In a simple approximation, the energy of the PL peak from a confined semiconductor can be written as follows:

$$E_{PL} = E_{Bulk} + \Delta E \tag{5}$$

Where E_{PL} (eV) refers to the energy at the PL peak, E_{Bulk} (eV) to the maximum of the signal for a bulk perovskite sample. The term ΔE describes the increased energy as a consequence of quantum confinement. The consistent increase in E_{PL} (3 nm: 2.44 eV, 5 nm: 2.41 eV, 10 nm: 2.38 eV, 60 nm: 2.37 eV, and 150 nm: 2.37 eV, Figure S7, Supporting Information) confirms the effective separation of perovskite layers and credibility of the sample fabrication. Notably, the 150 nm-perovskite emission spectrum shows a slight blue shift compared to the 60 nm-perovskite multilayers. Extended evaporation may result in $CsPb_2Br_5$ formation on the substrate due to decomposed powder, lacking an organic seeding layer. This is likely to encase $CsPbBr_3$, causing quantum confinement.

Of all reported evaporated perovskites, $CsPbBr_3$ is the most widely used in solar cells and LEDs where generally it is employed with a layer thickness in excess of 100 nm.[36,37] However, to date, thermally evaporated perovskite-organic multilayers have not yet been widely applied to optoelectronic devices, and correlations between the MQWs layers' thickness and their optical properties are still scarce.

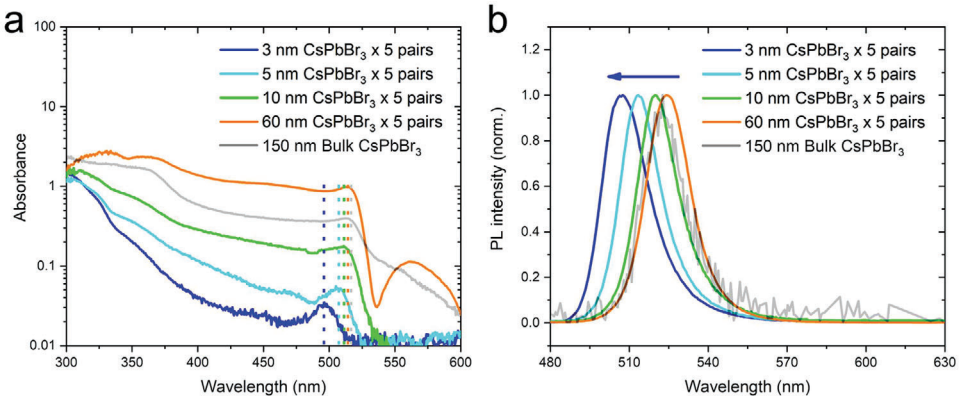

Figure 2. a) Absorbance and b) photoluminescence spectra of $CsPbBr_3$/TPBi multilayers (excitation wavelength 405 nm).

Therefore, we focused on multilayers employing thicker (60 nm) perovskite layers: **Figure** 3a–c, shows the PL spectra from architectures consisting of multilayers (5 stacks) employing a 60 nm $CsPbBr_3$ perovskite film and varying thicknesses of the TPBI layer, ranging from 75, 45 nm to 15 nm. While the 75nm-TPBi MQWs only shows spontaneous emission, stable ASE at room temperature is clearly observed for the multilayers with 45- and 15 nm-thick TPBi, with threshold decreasing from 207 and 72 μJ cm^{-2}, respectively (detailed specification is elaborated in Figure S9, Supporting Information).

This might be explained with enhanced internal reflection in thick TPBi layers, that can reinforce reabsorption in the perovskite in the multilayers thus increasing parasitic absorption.[38,39] To observe ASE, fast radiative recombination from a high charge carrier density is required, however, photon reabsorption redistributes the charge carriers and delays the recombination.

To verify this hypothesis, we performed transient PL characterization on the films using the time correlated single photon counting technique. Multilayers with 15-, 45-, and 75 nm-thick TPBi showed 104, 153, and 247 ps of PL decay time, respectively (Figure S10, Supporting Information). The increased PL lifetime can be explained by charge carrier re-distribution and subsequential slower recombination due to reabsorption, which is induced by thicker layers and is consistent with the suppression of ASE with thicker TPBi.[39] Finally, to investigate the photonic properties of the best performing MQW made of 5 stacks of repeating TPBi 15 nm/$CsPbBr_3$ 60 nm layers, we employed finite-difference time-domain (FDTD) method to simulate the structure, based on refractive index and extinction coefficient retrieved from ellipsometry measurements on $CsPbBr_3$ and TPBi (Figure S11, Supporting Information). **Figure** 4a shows the transmission and reflection spectra, where a broadband plane wave is sent to the normal direction of the film, two monitors are placed at the back and in front of the film as the schematic model as the inset in Figure 4a. Figure 4b shows the electric field of the stack, where dipoles are placed in the $CsPbBr_3$ layer, simulating the spontaneous emission. The simulation shows that light is effectively confined in the perovskite layers due to the refractive index difference between layers ($CsPbBr_3$-TPBi), and confirms that, upon proper design of the multilayered architecture, the intercalating organic layer can improve the ASE performance by increasing the photoexcitation efficiency of $CsPbBr_3$ as well as the density of photogenerated carriers within the heterostructure's wells.

3. Conclusion

In summary, perovskite-organic multilayers were successfully fabricated by sequential single-source evaporation, starting from mechanochemical synthesis of $CsPbBr_3$ perovskite powders via ball-milling. This intercalated organic layer suppresses defect

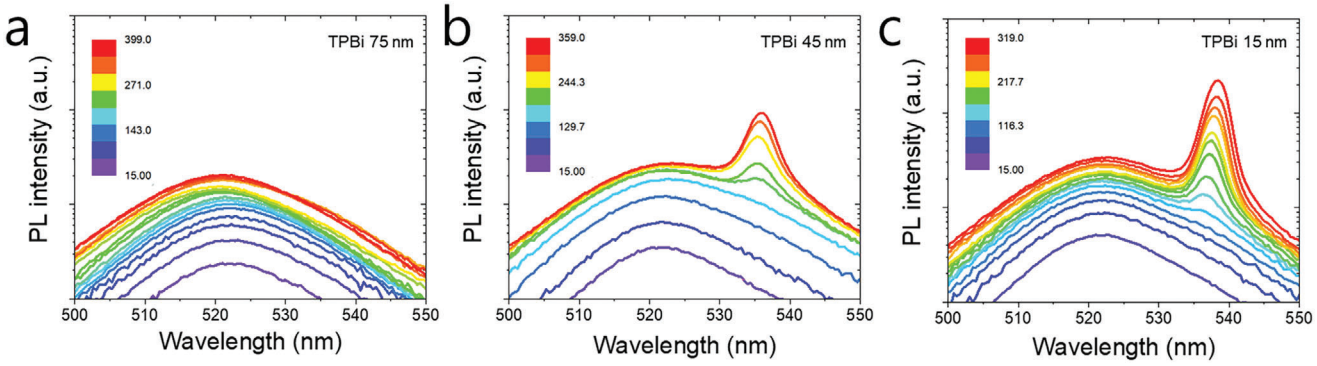

Figure 3. Amplified spontaneous emissions (ASEs) from five paired multilayers with a) 75 nm-, b) 45 nm-, and c) 15 nm-thick organic layers. (inset: excitation fluence, μJ cm^{-2}).

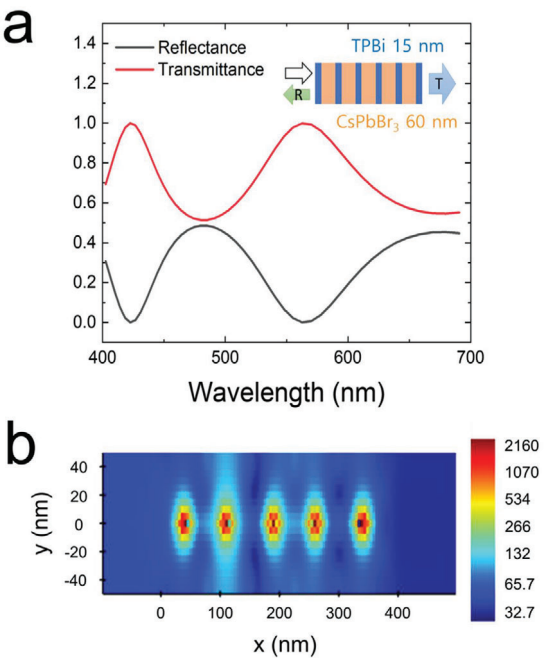

Figure 4. Numerical simulation of TPBi (15 nm)/CsPbBr3 (60 nm) stack. a) Transmission and reflection spectrum of the stack. (Inset: the schematic illustration of the stack) b) Simulated electric field in the stack.

states and improves the seeding of the evaporated perovskites stabilizing its 3D phase. Simultaneously, the heterostructure is shown to radically enhance the radiative recombination properties and, upon proper design of the multilayers' interlayer-thickness, ASE was achieved at room temperature under pulsed optical excitation. Our single-source evaporation strategy provides a simpler fabrication method (compared to perovskite co-evaporation) for the realization of perovskite multilayers and provides fundamental insights on the photophysical and photonic properties of such heterostructures that will be highly valuable to push their development toward lasing applications.

Supporting Information

Supporting Information is available from the Wiley Online Library or from the author.

Acknowledgements

S.-H.C. and D.C. contributed equally to this work. The authors acknowledge Jorge Ferrando for his technical support with the vacuum chambers. This project has received funding from the European Research Council (ERC) under the European Union's Horizon 2020 research and innovation program (grant agreement No 834431), from the Comunitat Valenciana (PROMETEU/2020/077) and from grants CEX2019-000919-M and PDC2021-121317-I00 project funded by MCIN/AEI/10.13039/501100011033 and the European Union "NextGenerationEU"/"PRTR". G.F. and A.P. acknowledge the funding from the European Union's Horizon 2020 research and innovation program through the ERC project SOPHY under Grant Agreement No. 771528, and D.C. through ERC project SUPER, grant agreement No 101040681. C.-S.W. acknowledges funding from the European Union's Horizon 2020 research and innovation program MSCA-ITN PERSEPHONe under Grant Agreement No. 956270. A.T. acknowledges funding from the European Union's Horizon 2020 research and innovation programme under the Marie Skłodowska-Curie grant agreement No 860553.

Conflict of Interest

The authors declare no conflict of interest.

Data Availability Statement

The data that support the findings of this study are available from the corresponding author upon reasonable request.

Keywords

amplified spontaneous emission, perovskite, single-source evaporation, thermal evaporation

Received: October 23, 2023
Revised: January 29, 2024
Published online: February 22, 2024

[1] M. Grätzel, *Acc. Chem. Res.* **2017**, *50*, 487.
[2] A. Fakharuddin, M. K. Gangishetty, M. Abdi-Jalebi, S.-H. Chin, A. R. M. Yusoff, D. N. Congreve, W. Tress, F. Deschler, M. Vasilopoulou, H. J. Bolink, *Nat. Electron.* **2022**, *5*, 203.
[3] L. Protesescu, S. Yakunin, M. I. Bodnarchuk, F. Krieg, R. Caputo, C. H. Hendon, R. X. Yang, A. Walsh, M. V. Kovalenko, *Nano Lett.* **2015**, *15*, 3692.
[4] S. H. Chin, J. W. Choi, H. C. Woo, J. H. Kim, H. S. Lee, C. L. Lee, *Nanoscale* **2019**, *11*, 5861.
[5] H. C. Woo, J. W. Choi, J. Shin, S. H. Chin, M. H. Ann, C. L. Lee, *J. Phys. Chem. Lett.* **2018**, *9*, 4066.
[6] Y. H. Kim, S. Kim, A. Kakekhani, J. Park, J. Park, Y. H. Lee, H. Xu, S. Nagane, R. B. Wexler, D. H. Kim, S. H. Jo, L. Martínez-Sarti, P. Tan, A. Sadhanala, G. S. Park, Y. W. Kim, B. Hu, H. J. Bolink, S. Yoo, R. H. Friend, A. M. Rappe, T. W. Lee, *Nat. Photonics* **2021**, *15*, 148.
[7] B. R. Sutherland, S. Hoogland, M. M. Adachi, C. T. O. Wong, E. H. Sargent, *ACS Nano* **2014**, *8*, 10947.
[8] C. Qin, A. S. D. Sandanayaka, C. Zhao, T. Matsushima, D. Zhang, T. Fujihara, C. Adachi, *Nature* **2020**, *585*, 53.
[9] A. L. Alvarado-Leaños, D. Cortecchia, G. Folpini, A. R. Srimath Kandada, A. Petrozza, *Adv. Opt. Mater.* **2021**, *9*, 2001773.
[10] C. Cho, A. Palatnik, M. Sudzius, R. Grodofzig, F. Nehm, K. Leo, *ACS Appl. Mater. Interfaces* **2020**, *12*, 35242.
[11] F. Deschler, M. Price, S. Pathak, L. E. Klintberg, D.-D. Jarausch, R. Higler, S. Hüttner, T. Leijtens, S. D. Stranks, H. J. Snaith, M. Atatüre, R. T. Phillips, R. H. Friend, *J. Phys. Chem. Lett.* **2014**, *5*, 1421.
[12] B. R. Sutherland, E. H. Sargent, *Nat. Photonics* **2016**, *10*, 295.
[13] C. Cho, T. Antrack, M. Kroll, Q. An, T. R. Bärschneider, A. Fischer, S. Meister, Y. Vaynzof, K. Leo, *Adv. Sci.* **2021**, *8*, 2101663.
[14] E. O. Odoh, A. S. Njapba, *Adv. Phys. Theor. Appl.* **2015**, *46*, 26.
[15] T. L. Leung, I. Ahmad, A. A. Syed, A. M. C. Ng, J. Popović, A. B. Djurišić, *Commun. Mater.* **2022**, *3*, 63.
[16] Y. Li, H. Zhou, M. Xia, H. Shen, T. Wang, H. Gao, X. Sheng, Y. Han, Z. Chen, L. Dou, H. Zhu, E. Shi, *Sci. Adv.* **2023**, *9*, adh0517.
[17] A. L. Alvarado-Leaños, D. Cortecchia, C. N. Saggau, S. Martani, G. Folpini, E. Feltri, M. D. Albaqami, L. Ma, A. Petrozza, *ACS Nano* **2022**, *16*, 20671.

[18] T. Antrack, M. Kroll, M. Sudzius, C. Cho, P. Imbrasas, M. Albaladejo-Siguan, J. Benduhn, L. Merten, A. Hinderhofer, F. Schreiber, S. Reineke, Y. Vaynzof, K. Leo, *Adv. Sci.* **2022**, *9*, 2200379.
[19] K. J. Lee, B. Turedi, L. Sinatra, A. A. Zhumekenov, P. Maity, I. Dursun, R. Naphade, N. Merdad, A. Alsalloum, S. Oh, N. Wehbe, M. N. Hedhili, C. H. Kang, R. C. Subedi, N. Cho, J. S. Kim, B. S. Ooi, O. F. Mohammed, O. M. Bakr, *Nano Lett.* **2019**, *19*, 3535.
[20] K. J. Lee, N. A. Merdad, P. Maity, J. K. El-Demellawi, Z. Lui, L. Sinatra, A. A. Zhumekenov, M. N. Hedhili, J.-W. Min, J.-H. Min, L. Gutiérrez-Arzaluz, D. H. Anjum, N. Wei, B. S. Ooi, H. N. Alshareef, O. F. Mohammed, O. M. Bakr, *Adv. Mater.* **2021**, *33*, 2005166.
[21] B. S. Kim, L. Gil-Escrig, M. Sessolo, H. J. Bolink, *J. Phys. Chem. Lett.* **2020**, *11*, 6852.
[22] M. Kroll, S. D. Öz, Z. Zhang, R. Ji, T. Schramm, T. Antrack, Y. Vaynzof, S. Olthof, K. Leo, *Sustain. Energy Fuels* **2022**, *6*, 3230.
[23] Y. El Ajjouri, F. Palazon, M. Sessolo, H. J. Bolink, *Chem. Mater.* **2018**, *30*, 7423.
[24] F. Palazon, Y. El Ajjouri, P. Sebastia-Luna, S. Lauciello, L. Manna, H. J. Bolink, *J. Mater. Chem. C Mater.* **2019**, *7*, 11406.
[25] M. Anni, S. Lattante, *J. Phys. Chem. C* **2015**, *119*, 21620.
[26] L. Lei, D. Seyitliyev, S. Stuard, J. Mendes, Q. Dong, X. Fu, Y. A. Chen, S. He, X. Yi, L. Zhu, C. H. Chang, H. Ade, K. Gundogdu, F. So, *Adv. Mater.* **2020**, *32*, 1906571.
[27] S. Cho, S. H. Yun, *Commun. Chem.* **2020**, *3*, 15.
[28] Y. Zhao, I. Yavuz, M. Wang, M. H. Weber, M. Xu, J. H. Lee, S. Tan, T. Huang, D. Meng, R. Wang, J. Xue, S. J. Lee, S. H. Bae, A. Zhang, S. G. Choi, Y. Yin, J. Liu, T. H. Han, Y. Shi, H. Ma, W. Yang, Q. Xing, Y. Zhou, P. Shi, S. Wang, E. Zhang, J. Bian, X. Pan, N. G. Park, J. W. Lee, et al., *Nat. Mater.* **2022**, *21*, 1396.
[29] B. Yang, D. Bogachuk, J. Suo, L. Wagner, H. Kim, J. Lim, A. Hinsch, G. Boschloo, M. K. Nazeeruddin, A. Hagfeldt, *Chem. Soc. Rev.* **2022**, *51*, 7509.
[30] M. Reufer, J. Feldmann, P. Rudati, A. Ruhl, D. Müller, K. Meerholz, C. Karnutsch, M. Gerken, U. Lemmer, *Appl. Phys. Lett.* **2005**, *86*, 221102.
[31] M. H. Park, S. H. Jeong, H. K. Seo, C. Wolf, Y. H. Kim, H. Kim, J. Byun, J. S. Kim, H. Cho, T. W. Lee, *Nano Energy* **2017**, *42*, 157.
[32] H. Cho, S. H. Jeong, M. H. Park, Y. H. Kim, C. Wolf, C. L. Lee, J. H. Heo, A. Sadhanala, N. S. Myoung, S. Yoo, S. H. Im, R. H. Friend, T. W. Lee, *Science* **2015**, *350*, 1222.
[33] M. Li, P. Huang, H. Zhong, *J. Phys. Chem. Lett.* **2023**, *14*, 1592.
[34] E. Ugur, M. Ledinský, T. G. Allen, J. Holovský, A. Vlk, S. De Wolf, *J. Phys. Chem. Lett.* **2022**, *13*, 7702.
[35] D. Di, K. P. Musselman, G. Li, A. Sadhanala, Y. Ievskaya, Q. Song, Z. K. Tan, M. L. Lai, J. L. MacManus-Driscoll, N. C. Greenham, R. H. Friend, *J. Phys. Chem. Lett.* **2015**, *6*, 446.
[36] J. Li, R. Gao, F. Gao, J. Lei, H. Wang, X. Wu, J. Li, H. Liu, X. Hua, S. (Frank) Liu, *J. Alloys Compd.* **2020**, *818*, 152903.
[37] P. Du, J. Li, L. Wang, L. Sun, X. Wang, X. Xu, L. Yang, J. Pang, W. Liang, J. Luo, Y. Ma, J. Tang, *Nat. Commun.* **2021**, *12*, 1.
[38] C.-H. Chen, C.-L. Liu, S.-T. Chung, *Opt. Lett.* **2013**, *38*, 5315.
[39] J. Navarro-Arenas, I. Suárez, V. S. Chirvony, A. F. Gualdrón-Reyes, I. Mora-Seró, J. Martínez-Pastor, *J. Phys. Chem. Lett.* **2019**, *10*, 6389.